

# ON THE SIMULATION OF REAL FIRE FOR POST FIRE RESISTANCE EVALUATION OF STEEL STRUCTURES

## ABSTRACT

Post fire resistance assessment of industrial steel structures is of prime importance to companies having to deal with such accidental situations. Most of the time, the structure or at least a major part of it still stands. Being able to quickly assess the temperature it was once submitted to is very important to re-evaluate its load-bearing capacity. The latter is to help take wise decisions regarding its dismantling or replacement and to avoid unnecessary delays during which the industry can no longer carry out its business. After being heated during a certain time, any kind of structure and material can be affected by locked in forces for continuous structures and possible material deterioration. Developing or simulating a real fire that is at least in agreement with visual observations or tests done on the structure after the fire, is the only way to assess the remaining resistance and thus reliability of the structure. The use of a standard heating curve is inappropriate to deal with post-fire situations and there is a clear need to establish the fire exposure characteristics in order to estimate the residual properties of a structure that survived the event. This paper aims to evaluate existing methodologies for post-fire assessment of structures having been submitted to a real fire. Results from models built with very sophisticated tools (Computational Fluid Dynamics) are compared to very simple and quick two-zone models (in Ozone). One well instrumented academic test is firstly used to compare these techniques. Then, two additional case-studies are used to illustrate that it is possible to simulate a fire with all its intrinsic features with relatively simple tools and to illustrate the influence of the chosen model on the structural response.

**Keywords:** *Full-scale fire test, Real fire, Compartment fire, FDS simulation, Post fire evaluation.*

## 1 INTRODUCTION

Post fire load bearing assessment of industrial structures is of high economic importance for most industries, who unfortunately have to deal with such accidental events. The economic losses due to a fire can be in the form of goods or equipment and, sometimes, part of the building also loses its resistance. Through reliability methods based on numerical evaluation of the temperature development in the load-bearing structure, the impact of the fire on the overall building resistance can be assessed [1]. In many cases, the structure exposed to the fire still stands and can be reused. And, therefore, the financial consequences are partially limited. It is evident that highly deformed elements which affect the functionality of the building need to be replaced, and there is, in such case, no need for this kind of time-consuming analyses. Neither is this the case for small connecting components, such as bolts, which are easy to replace [2]. However, the opposite is true for principal bearing elements, non-load-carrying costly elements and elements which are difficult to replace out of practical reasons. It is also of prime importance to be able to relatively quickly calculate the remaining load-bearing capacity and reliability of the structure to help take wise decisions regarding its dismantling or replacement and to avoid unnecessary delays during which the industry can no longer carry out its business. However, it is not possible to determine the performance of these structural components by testing techniques. Only indications about the results of the thermal action can be obtained (mostly via an indirect way), but to assess the residual bearing capacity of a structure,

a calculation is needed. To make this possible in a scientifically sound manner, more information is needed about the fire evolution (heating and cooling) and therefore a numerical reproduction of the fire is essential. This reproduced fire can be calibrated (benchmarking) against observations and will deliver the needed information for structural post-fire assessment.

To obtain an idea of the temperatures reached in the structural elements during and after the fire, measurements (based on tests), photos and videos can be of great help. Unfortunately, most of the time, only some external visible parameters can be obtained such as the melting or degradation temperature of the materials included in the building or information obtained by the fire brigade. The accuracy of such an evaluation technique is high when the considered material is fully accessible and not influenced by the surrounding environment. On the contrary, the temperature reached by non-visible parts of the structure (like the upper flange of a beam for example) can rarely be accurately estimated. To fill this lack of knowledge, a simulation of the effect of a real fire on the structure can be done by the aid of several techniques based on a number of assumptions, such as parametric fires, local fires, Two-zone models or through the use of Computational Fluid Dynamics (CFD). However, modelling the effects of real, even well characterised, full-scale fire on steel structures using numerical techniques remains today quite a challenge and only a few scientific references can be found on this topic such as [3] and [4]. While a few case-studies of industrial buildings submitted to real fire scenarios are available in the literature, for example [5], there is a lack of studies coupling numerical models with on-site observations during and after the occurrence of a fire. In addition, although different simulation techniques have already been compared in the past [6], so far, they are not verified against test data after the occurrence of the real fire [7].

This article presents such a more complete and enhanced analysis. It is partially based on [8], which can be seen as a first, however still limited, exploration of the topic. After an in-depth investigation of a well described full-scale experiment (limited till the thermal part), two real fire case-studies are modelled and used to illustrate the methodology to study a structure in post-fire conditions. Only the latter cases are worked out until the mechanical response, as it was only there relevant. After the fire, comparisons are made between calculated quantities with other quantifiable information (provided by the fire brigade for example) to evaluate the accuracy of the proposed simulation. The model can be helpful to understand what has happened during the fire and how the temperature distribution in a studied enclosure developed. Then, based on the post fire material characteristics, the remaining load bearing capacity of the building can be assessed. The advantage of this theoretical evaluation is clear: due to several practical reasons, uncertainties on the structural evaluation can be significantly reduced and it can help focussing on the most sensitive locations on site.

The proposed methodology is schematically depicted in Figure 1, post-assessment by the aid of visual observations or information obtained through the fire brigade is of prime importance to assess the accuracy of the numerical model. The knowledge of the thermal load on a structure and its initial boundary conditions [9] are the main parameters to start with, during the structure resistance verification after the fire. As already mentioned, to assess the validity of the numerical model, several types of (visual) observations can be used. In some cases, only some basic information is available and scientific hypotheses on the maximum attained temperatures must be supported by additional material tests. These tests can take the form of an evaluation of the mechanical characteristics or, as it is the case of steel, of changes in crystal structure [10].

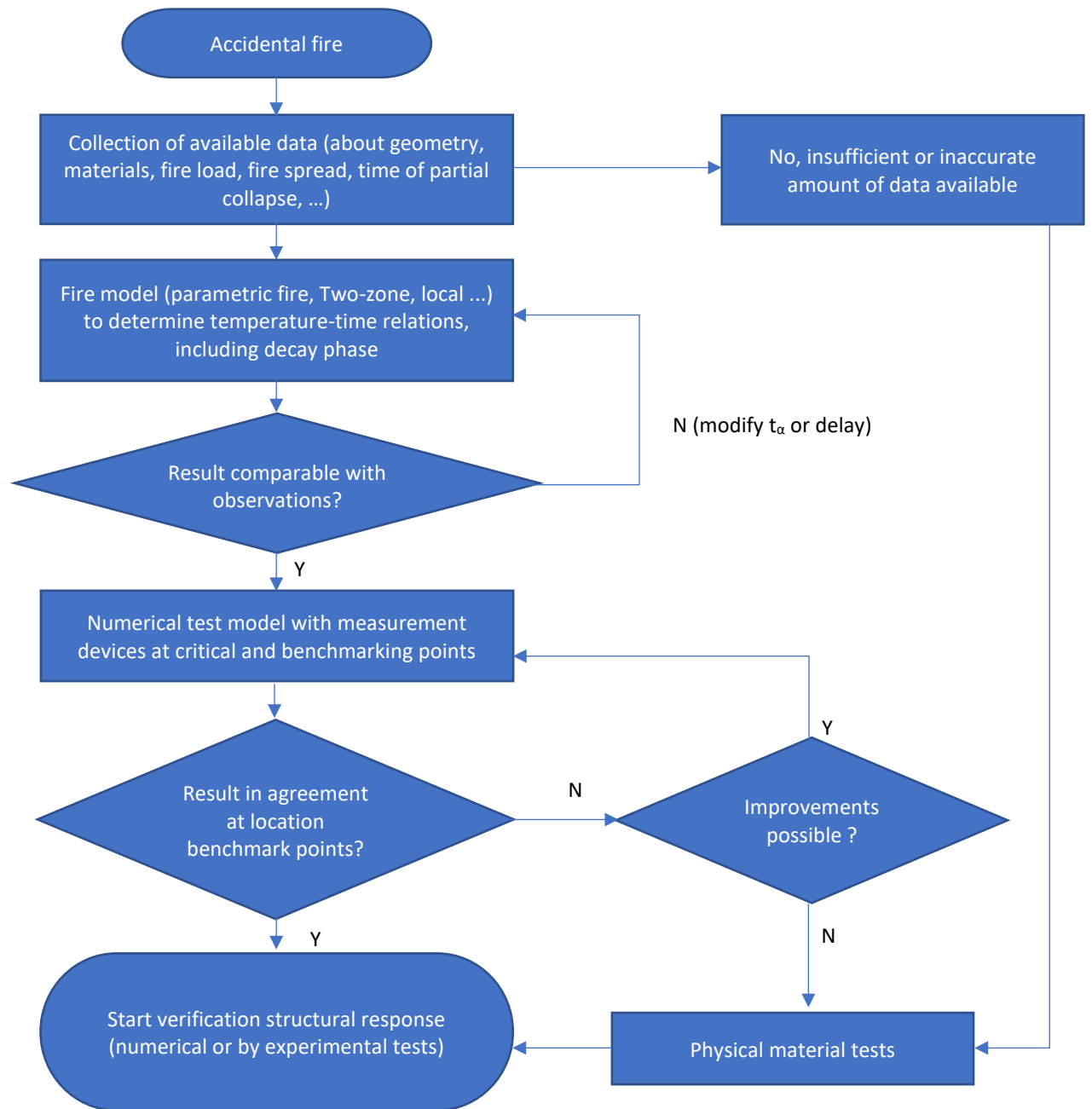


**Figure 1. Flow chart**

The methodology is validated using one first example and then further illustrated using two real case-studies. The first one firstly focusses on a steel portal frame which was subjected to, an experimental and therefore instrumented, real compartment fire for which one has access to all the information during and after the fire [11]. In addition, two additional real (i.e. non-academic) local fires after which the structure survived the fire are studied by means of the same approach.

## 2 REFERENCE FULL-SCALE FIRE TESTS

Only very few well instrumented and controlled studies of industrial structures are available to study the accuracy of simulations of full-scale real fires. On several occasions, the carried test did not lead to the expected conclusions because of environmental parameters. For example, during a previously executed full-scale fire test in Belgium in collaboration with KU Leuven, see Figure 2, it was not possible to foresee the location of collapse due to a change in the wind direction during the test [12].

In France, a partially built warehouse was set into fire in the scope of a National project named Flumilog [13] and, there too, a strong influence of the wind was noticed. An extensive study [14] made in Germany was dealing with the missing or failing intumescent coating in narrow spaces between outer flanges and wall cladding or trapezoidal steel decking. They executed several fire tests on columns and beams, comparing the temperatures to investigate the behaviour of a non-expanding or absent intumescent coating. The conclusions drawn from this study [15] were demonstrated by a numerical study executed with Fire Dynamics Simulator (FDS) [16].



**Figure 2. Overview of full-scale fire experiments; KU Leuven [12], Flumilog [13] and Tongji [17].**

Only recently, new data on the experimental study of a full-scale fire test on a steel portal frame were published [11]. This study was executed at the Tongji university, which is the reason why it will be named it the Tongji-experiment in the present paper. Photos of the tested building were taken each five minutes, hence there is a possibility to compare the simulations of the present study against visual observations during the fire. Temperature data at four locations inside the compartment were registered. Thermocouples were placed at four levels on columns, beams and rafters, the measurements of which were published in [11]. The fire load was obtained via wooden cribs and is therefore well characterised. Based on this information, a model with local fires, a Two-zone model and a FDS version 6.7 model [18] were built to simulate the effect of the fire on the building. Section 3 describes the Tongji experiment in detail. In the following section (Section 4) of this paper, several procedures are compared with each other and their results are validated against the aforementioned well instrumented fire test (Tongji experiment). In section 5 however, two real fire case-studies are included to illustrate the applicability of the proposed methodology.

### 3 THE TONGJI EXPERIMENT

#### 3.1 Geometrical information

An extensive description of the experiment and the recorded measurements can be found in [11] and [17], some data necessary to understand the next steps of this paper will be repeated here. As illustrated in Figure 3 (a), two steel frameworks were erected with a span of 12 m, a roof edge at 5.4 m and a roof ridge at 5.8 m. The structure's skin was made of sandwich panels i.e. rock wool insulation core inserted between two thin-walled steel sheets. An inner partition wall was added with a fire rate of 3 hours (ISO834 fire) with a spacing of 0.3 m on top and 0.15 m on its sides (which allows free expansion but has been smoke proof finished) as well as a door of 1.0 by 1.8 m. By doing so, a fire compartment (with one window opening) of 4.0 by 6.0 m was created. The authors do not provide information on the type of window that was used. In the present study, the authors first assume that the window is open in order to get a first estimation of the temperature development. Then, single glazing will be considered together with the following assumptions, based on the Luxemburg rules for Fires Safety Engineering purposes [19]: in combination with a smoke temperature of 100°C or 250°C, the window opening reaches 50% or 90%, respectively. It is worth pointing out at this stage that it was already demonstrated in [20] that the stress distribution in the glass does not fluctuate a lot between 250°C and 400°C, and therefore neither does the failure risk. In the compartment besides, a door opening of 2.0 by 3.0 m was included.

$$O = \frac{A_v \sqrt{h_{eq}}}{A_t} = \frac{1 \cdot 1.8 \sqrt{1.8}}{2 \cdot 4 \cdot 6 + 2 \cdot 5.6 \cdot (4 + 6)} = 0.015 \text{ m}^{1/2} \quad (1)$$

The factor  $O$  is lower than the minimum bound of  $0.02 \text{ m}^{1/2}$  recommended in [23]. Due to the glass breaking however, the window opening reaches 90% of its theoretical surface, hence the opening factor increases up to  $0.02 \text{ m}^{1/2}$  after failure of the glass. Eq. (1) then becomes Eq. (2).

$$O = \frac{A_v \sqrt{h_{eq}}}{A_t} = \frac{(1 \cdot 1.8 + 1 \cdot 0.8) \sqrt{1.49}}{2 \cdot 4 \cdot 6 + 2 \cdot 5.6 \cdot (4 + 6)} = 0.020 \text{ m}^{1/2} \quad (2)$$

### 3.2 Fire load

5

the reference article is that the authors used the gross volume of the piles instead of its net volume. With a floor area of only 24 m<sup>2</sup>, the fire load density is 40425/24 = 1684 MJ/m<sup>2</sup>.

$$Q = n \cdot s \cdot \frac{l}{2} \cdot (W + L) \cdot a^2 \cdot \rho \cdot H_u = 4 \cdot 15 \cdot 10 \cdot (1.5 + 2) \cdot 0.05^2 \cdot 440 \cdot 17.5 = 40425 MJ \quad (3)$$

The measured heat release rate (HRR) was about 5 MW per pile [11], a similar value is obtained by the application of the Annex E of Eurocode 1 [23]. However, in [11], it is stated (although without further explanation) that the total HRR will be 4 · 5 or 20 MW. With a ventilation-controlled fire, this will not be the case and the prescriptions of the Eurocode 1 limit the HRR to the value of Eq. (4):

$$Q_{vent} = 0.10 \cdot m \cdot H_u \cdot A_v \cdot \sqrt{h_{eq}} = 4.45 MW \quad (4)$$

where  $m$  = combustion factor (0.8),  $H_u$  = net calorific value of the wood,  $A_v$  = 2.6 m<sup>2</sup> and  $h_{eq}$  = 1.49 m as before.

## 4 VALIDATION OF THE NUMERICAL MODELS

### 4.1 Parametric fire

The parametric fire is a way to develop a temperature-time relationship [21], [22] based on a semi-empirical formulation. Variables as the ventilation characteristics i.e. the area of vertical opening  $A_v$  and the opening factor  $O$ ; the fire load  $q_{t,d}$  related to the total area  $A_t$  of enclosures; the building properties through the effusivity  $b = \sqrt{\rho c \lambda}$  are involved, where  $\rho$ ,  $c$  and  $\lambda$  are the material density, specific heat and conductivity respectively. This nevertheless remains a so-called engineering model [23] i.e. not based on gas properties, energy and mass balance equations. As long as the ratio of the vertical openings and the total surface of the enclosures, the equivalent height (i.e. the weighted average of all vertical openings), the fire load  $q_{t,d}$  and the thermal properties (i.e. the effusivity) are kept constant, the final result remains constant as well.

In the reference article [11], a simulation was made using a parametric fire method even though the criterium of maximum height (4 m following [24]) was not fulfilled. Additionally, the effusivity  $b$  indicated by the authors (1500 J/m<sup>2</sup>s<sup>0.5</sup>K) seems high considering that the roof and 3 out of 4 walls are made of stone wool sandwich panels with an inner 0.5 mm steel sheet. Also, after 20 minutes of fire, a maximum temperature of 1107 °C is reached which indicates that the fire is fuel-controlled, and considering the opening factor given by Eq. (2) and the fire load indicated in the article (i.e. 3413 MJ/m<sup>2</sup>) we could conclude that there had been inaccuracies reported in the paper. To agree with the formulation from [24] and the evaluations presented in section 3, the parametric fire was recalculated based on the thermal properties presented in Table 1 and the variables listed below:

- A surface weighted effusivity of 403 J/m<sup>2</sup>s<sup>0.5</sup>K, based on and the values from Table 1 instead of 1500 J/m<sup>2</sup>s<sup>0.5</sup>K provided in [11],
- An opening factor  $O = 0.02 \text{ m}^{1/2}$ , see Eq. (2),
- An equivalent height  $h_{eq} = 1.49 \text{ m}$ ,
- A fire load  $q_{f,d}$  of 1684 MJ/m<sup>2</sup> (see section 3.2) in combination with a combustion factor  $m = 0.8$  and a natural “dry” wood moisture content  $\underline{u}$  of 15% expressed as percentage of the dry weight. Reworking  $q_{t,d}$  with these new assumptions, this delivers 173 MJ/m<sup>2</sup> instead of 525 MJ/m<sup>2</sup> as in [11].
- A medium fire growth rate or  $t_{lim} = 20 \text{ min}$ , the fire is however ventilation controlled. The opposite is assumed in [11] and, as mentioned, very unlikely to happen.

**Table 1 Material characteristics for the thermal models**

Description	Material	Thickness [m]	Conductivity $\lambda$ [W/mK]	Specific heat $c$ [J/kgK]	Density $\rho$ [kg/m <sup>3</sup> ]	Backing
Floor	Concrete	0.15	1.6	1000	2300	Exposed
Fire wall	Cellular concrete	0.20	0.14	840	550	Exposed
Profile	Steel	0.01	45	600	7850	Exposed
Sheet	Steel	0.0005	45	600	7850	Exposed
Insulation	Wool	0.075	0.037	1030	60	Exposed

Under these assumptions, the predicted maximum temperature in the heating phase of the gas  $\theta_{\text{Max}}$  equals to 1135 °C which is remarkably close to the maximum temperatures (1140-1190°C) measured by the highest thermocouple #6 on the temperature trees, see Figure 3. It is also possible to generate a temperature-time relationship based on the equations proposed in [24], and this will be discussed later on together with the results of the two-zone model in Figure 7. It is worth pointing out here that the parametric fire only describes the fully developed phase (as in the standard fire), and that it was assumed that this phase only started after 12 minutes according to [11]. This will be an important information when we will be comparing different time-temperature curves later on in this paper.

## 4.2 Local fire Model

Local fires are considered as severe accidental situations if the fire is situated under a supporting beam, next to a column or out of the opening of a (sub-)compartment (Annex B of [24]). Less severe cases can advantageously be modelled through the Heskestad model (during which it is assumed that the flames do not touch the ceiling) or the Hasemi models (in which the flames are touching the ceiling). For the Tongji experiment, it can be assumed that the behaviour of the four “piles” of interlaced and layered sticks (or cribs) could be modelled using four separate local Hasemi-fires. In the case of the so-called Hasemi fires, according to [24], the superposition principle is valid. So, a spatial distribution of the heat fluxes can be obtained where, at each location, the influence of several heating sources may be cumulated. This led to the idea of simulating the compartment fire of the Tongji experiment by the aid of four localised fires. However, it should be recognised that this is not a local fire in the meaning of Annex C of [24] where a flux loss due to the temperature of the section towards a cold (20°C) environment should be taken into account. In this case-study, the fire is fully developed in the compartment with a more or less uniform gas temperature. Re-emission of heat will take place from the section towards the relatively hot compartment temperature.

To model the fire, the wooden cribs were transferred to cylindrical volumes with the same surface (equivalent diameter of 1.96 m at 1 m above the ground) and a 5MW source for each. The fire height is taken equal to 1 m from the top of the wood pile. Due to the quite short duration of the fire, it is assumed that the volume of wood was not completely consumed (conservative assumption with a combustion factor equal to 0.8). A flame length of 5.08 m was found by following the guidelines of [24] and the heat flux received by the fire exposed unit surface area at the level of the ceiling could be calculated, as depicted Figure 4. It was noticed that, even for a clear compartment fire (one-zone), the heat flux greatly varies

Based on the position of the temperature trees, see Figure 3, it is obvious that the highest temperature should be measured at C# followed by B# and, due to symmetry, it will be more or less equal at A# and D#. According to [11], the measured thermocouple temperatures are indeed the highest at C# (1190°C) and more or less equal for the three other positions (maximum 1160°C for A# and 1140°C for B# and D#).

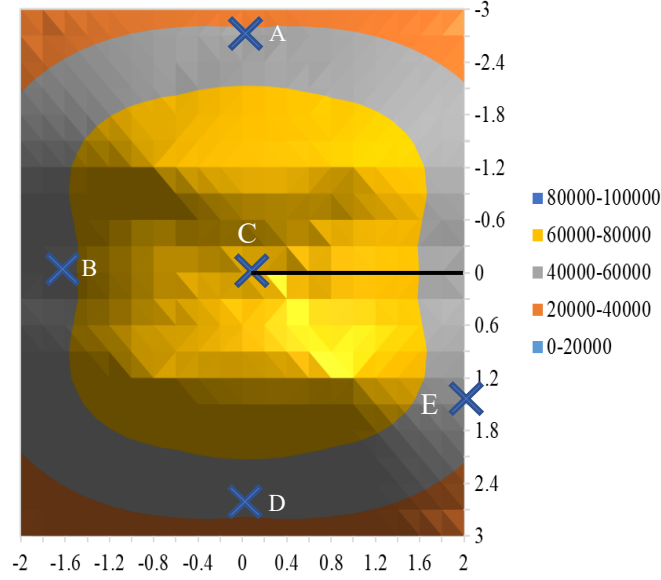


**Figure 4.** Distribution of the heat flux ( $\text{W/m}^2$ ) received by the fire exposed unit surface area of the ceiling in the left compartment in Figure 3 (a) of dimensions 4 x 6 m

Assuming a steady-state situation which makes that the net heat exchange ( $\dot{h}_{net}$ ) will be limited after 19 minutes of fire, Eq. (5) becomes approximately valid. By the aid of the heat flux  $\dot{h} = 74 \text{ kW/m}^2$  for C# from Eq. (5), a minimum material temperature  $\theta_m$  can be calculated, which reaches  $1314^\circ\text{C}$ . Depending on the compartment temperature, the material temperature can be calculated as depicted in Figure 5. The hot gas temperature  $\theta_g$ , which do not interfere in Eq. (5), is also given in Figure 5.

$$\dot{h}_{net} \approx 0 = \dot{h} - \alpha_c(\theta_m - \theta_{comp}) - \Phi \cdot \varepsilon_f \cdot \varepsilon_m \cdot \sigma \cdot ((\theta_m + 273)^4 - (\theta_{comp} + 273)^4) \quad (5)$$

Where  $\dot{h}_{net}$  = net heat flux,  $\alpha_c$  = convective heat flux =  $35 \text{ W/m}^2\text{K}$ ,  $\theta_m$  = temperature of the material,  $\theta_{comp}$  = temperature in the compartment, shadow factor  $\Phi = 1$ , the emissivity of the flames  $\varepsilon_f$  or the material  $\varepsilon_m$  are respectively equal to 1 or 0.7 [25], and  $\sigma$  is Boltzmann's constant.

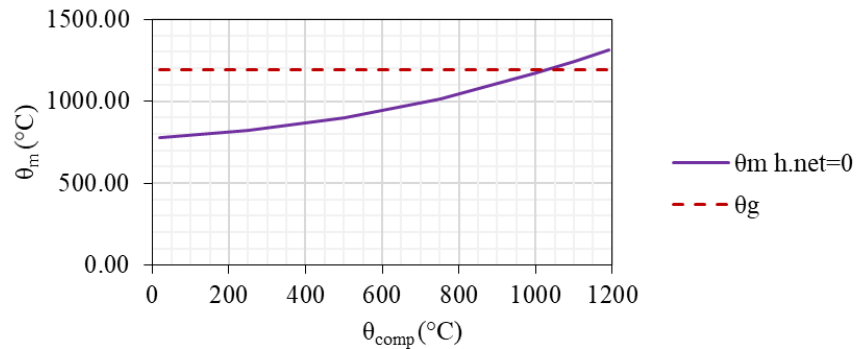


**Figure 5.** Material temperature in function of the compartment temperature.

Starting from a compartment temperature of roughly  $1000^\circ\text{C}$ , the steel temperature in the vicinity of the plume becomes higher than the one obtained based on the gas temperature. In the experiment, this condition was met at all thermocouple positions. Hence the temperature of the ceiling impinged by the heat flux of the Hasemi fire model will always be higher than the one of the gas temperature. Considering the predicted values at the ceiling level, the obtained average heat flux is  $57 \text{ kW/m}^2$ , with a standard deviation of  $14 \text{ kW/m}^2$ . However, this only represents a minor difference in the temperature range. By using the variation of the predicted values along the black line indicated in Figure 4 (i.e. 47 to  $74 \text{ kW/m}^2$ ), the temperature of a steel element against the ceiling can be obtained, see Figure 6.



The temperature is decreasing from 1314°C in the centre of the compartment to 1271 °C in the upper edge of the compartment, which is a rather low variation compared to the variation in heat flux. At the column locations, this decreases further to 1239°C. Unfortunately, temperatures are only measured on each column at 400 mm below the ceiling. Figure 3 shows values up to 1200 °C measured at column #4.

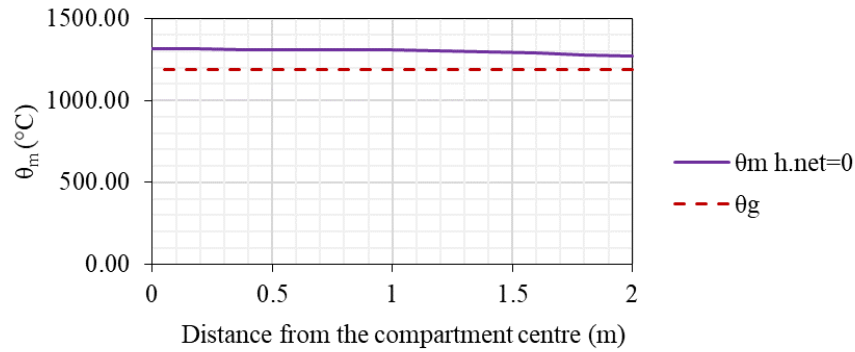


**Figure 6.** Material temperature in function of the distance to the compartment centre.

For this relatively modest case-study, the simple model in which the effects of 4 local fires were summed, provides quite accurate results. Nevertheless, presently, the material temperature was a known parameter and that is, in reality, not evident at all to guess it based on visual observations. However, if the temperatures would be available (through the use of another model for example), the spatial distribution of the heat fluxes is of high interest for the evaluation of the structural connections for example. It should be highlighted that these local fire models do not involve ventilation factors nor the thermal properties of walls or fire growth rates. To increase the accuracy for wider spaces, a combination of local fire models together with results obtained with a two-zone model should be considered [24].

### 4.3 Two-zone model

The case-study is outside the application range of a parametric fire due to the compartment height (5.4m instead of 4 m) and the rudimentary approximation consisting of superimposing four local fires is somewhat disputable. For these reasons, advanced fire models seem to be more appropriate to model this case-study. A simulation of the experiment by a Two-Zone model using the well-known Ozone software version 3.0.1 [26] was carried out. This model automatically becomes a 1-zone model if one of the following four criteria is met: the upper layer temperature is  $\geq 500^\circ\text{C}$ ; the combustible is engulfed in the upper layer and the upper layer temperature is  $\geq$  the ignition temperature of  $300^\circ\text{C}$ ; the interface height is  $\leq 0.2$  of the compartment height or at least the combustion area is  $\geq 1/4^{\text{th}}$  of the floor surface. Materials used in the model can be found in Table 1.

A user-defined fire characterised by the previously described geometry of the fire compartment was introduced, with a  $t_a$  of 5 min (300 s), a heat release rate of  $500 \text{ kW/m}^2$ , a fire load of  $1684 \text{ MJ/m}^2$  and a danger of fire activation equal to 1. The temperature of the upper layer (Ozone) and heat release rate (HRR) are respectively presented in Figure 7 and Figure 10.

A comparison between the visual observations during the test and those preliminary calculations was also made. It shows that 5 minutes after ignition, the fire was seriously developing but that the glazing of the window was still intact. In other words, the flashover occurs 5 min after ignition, despite the intact glazing. The Ozone calculation leads to a fully developed fire after only 1 min seen that, at that time, it automatically switched from 2 to 1 zone.

As for the post fire simulations, it can be noticed from Figure 7 (a), (Ozone 500s), where the Ozone upper layer temperatures and the measured steel temperatures in the tree #A (Figure 3) are provided, that the tool is appropriately predicting the smoke temperature. Note that, the Ozone temperature-time relation is shifted by 8.33 minutes (500 s) which is the ignition time (see dotted vertical line in Figure 7) and that the smoke temperature is compared to the steel temperature causing a slight decrease. The visual observations become rather important to define this so-called shift. Indeed, since glazing is still intact after 13.33 min (ignition time + 5 min), the smoke temperature at that moment should still be around 250°C i.e. the failure criteria for glass. Using Ozone, exceeding 250°C happens 4.77 min after ignition.

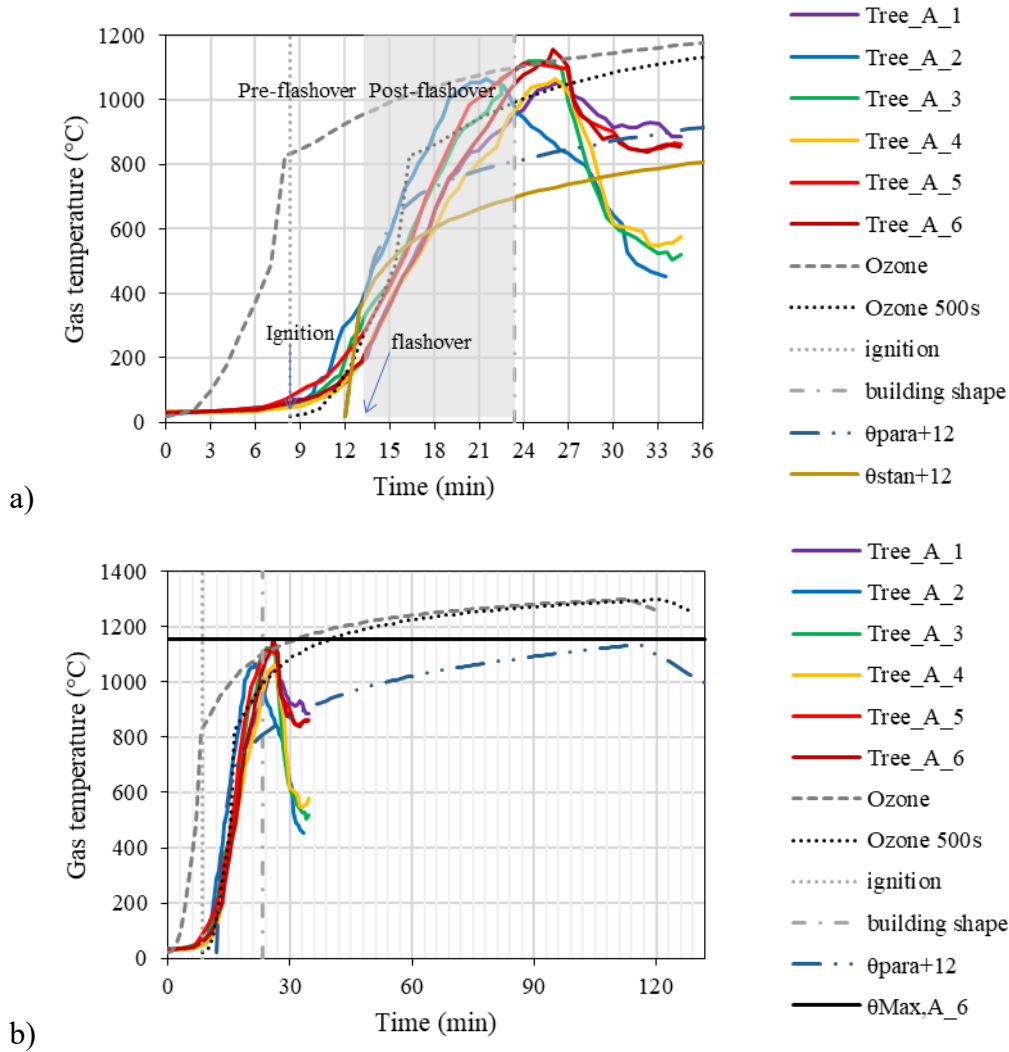


**Figure 7. Measured temperature development by thermocouple tree A# [11] together with the Ozone evaluation of the upper layer temperature TU a) till collapse of the building and b) till start of cooling phase without a collapse**

On the one hand, the smoke temperature calculated by Ozone seems to be relatively accurately predicting the growth phase, with some advance for thermocouples #A1 and #A4 and some delay for the other thermocouples. On the other hand, this is not the case for the parametric fire  $\theta_{para}$  nor the standard fire  $\theta_{stan}$ , both being delayed by 12 minutes as mentioned before. As shown in the whole temperature-time relationship however, the parametric fire does predict the maximum temperature more accurately, see Figure 7 (b). After 15 minutes of fire after ignition, a peak temperature of 1100 °C is measured as can be seen in Figure 7 (a). Moreover, the structure starts to fail, the wall cladding

tears apart leading to an extra amount of oxygen at that location with higher HRR and temperatures. It is also clear that, after 19 minutes of fire, the shape and volume of the compartment have drastically changed, see Figure 8.



**Figure 8. Tongji experiment at failure time [17]**

Due to the extra amount of oxygen and the changes in shape, the interesting time range is limited to about 15 minutes and definitely lower than 19 minutes after fire ignition [17], it is the area shaded in light grey in Figure 7.

After a thorough study of the articles [11] and [17], which both describe the same experiment, it came out that the reported measured steel temperatures before 13.33 min were different. After feedback of the authors, it became clear that the results as they are presented in the journal article are more reliable, which is why the findings hereafter are based on this reference [11].

## **4.4 FDS Model**

FDS or Fire Dynamic Simulator [18] is a widely used powerful tool for the description of the fluid behaviour in case of fire. Through the use of computational fluid dynamics, it is possible to go further in detail in the simulation although the use of such tool requests much more information to describe the fire and the system boundaries and it is, most of the time, time consuming. In [6], some comparison was already made between predictions based on FDS or on a local Heskestad fire. This study is however looking at a local fire rather than a compartment fire as it is presently the case.

### **4.4.1 General introduction to the model**

The smallest dimension of the wooden cribs is 50 mm. For that reason, the minimum mesh size was herein chosen equal to 50 mm. A mesh sensitivity check was executed with cell sizes equal to 100 or 150 mm and the comparison will be shown later on in this section. The FDS version 6.7 [18] was used. The numerical domain was limited to the combustion area except for the wall with an opening, where an extension of 1.5 m outside the building was considered to assess the interaction with the building's environment. The geometry of the model is shown in Figure 9.

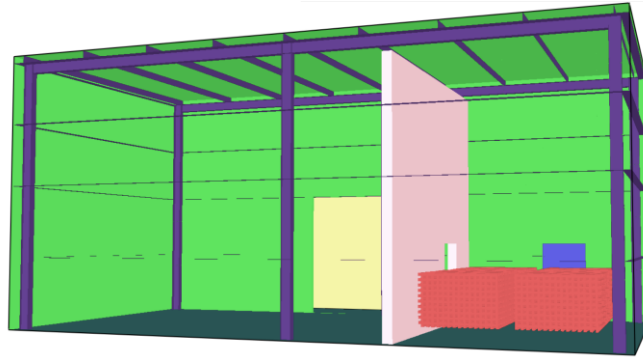


**Figure 9. FDS Model of the structure, with view on the fire load, window, door and gate**

The floor is made of concrete, sandwich elements are used for the walls, the roof and the boundaries of the open space next to the opening. Standard material characteristics were collected from the literature as presented in Table 1 since they are not provided in [17]. After 19 minutes of fire, the compartment geometry abruptly changes due to the failing structural elements, which is why the comparisons should be stopped after this time. Most importantly, the real reason is that the topic of this research focusses on the assessment of the (eventually) remaining post fire load bearing capacity. Nevertheless, the simulation reached a time period of 36 min and it was possible to see if the cooling phase with a changing geometry could also be properly modelled.

#### 4.4.2 Evolution in time of the fire

The global physical reaction of the wooden cribs was introduced as  $C_{3.4}H_{6.2}O_{2.5}$  with a soot yield of 0.015 and a heat of combustion equal to 17.5 MJ/kg. No attention was paid to travelling fire due to the relatively small size of the compartment. A first simulation was used as an upper bound: the combustion product develops the highest possible HRR. The amount of combustible energy was previously calculated as 40425 MJ. In the assumption of a linearly increasing heat over a period of 1440 s (time of maximum reached temperature in the compartment) and decreasing over 2160 s, the averaged energy over time is 22458 kW. This is more or less the description of a fuel-controlled fire with a quadratic growing stage as mentioned in [24] with the formulation of Eq. (6).

$$Q = \left(\frac{t}{t_\alpha}\right)^2 \text{ in MW} \quad (6)$$

Where  $Q$  is the rate of heat release in MW,  $t$  is the time after ignition in s and  $t_\alpha$  the time needed to reach a rate of heat release of 1MW according to [24].

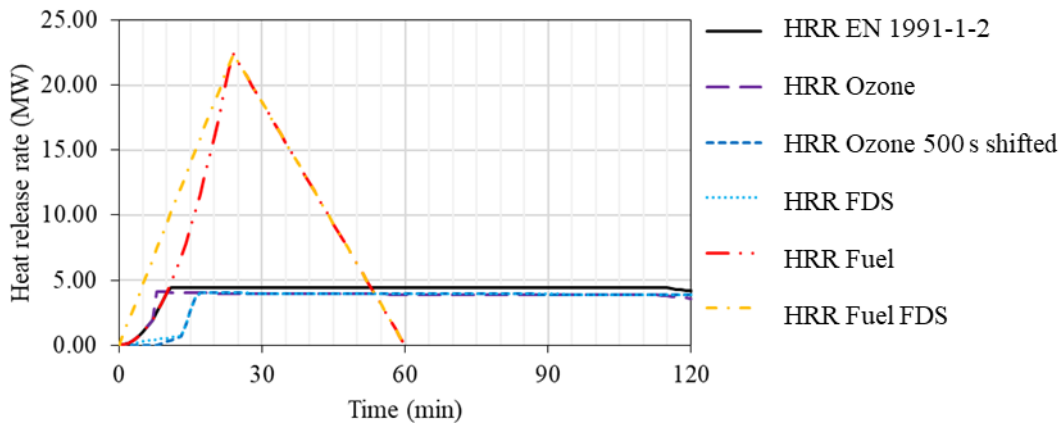


**Figure 10. HRR obtained by Ozone, EN1991-1-2 or a fuel-controlled fire**

After reaching the peak value, a linear decrease is assumed. The difference between a quadratic increase using Eq (6) with a  $t_a = 5$  min (300 s -moderate growing rate) and a linear approach can be seen in Figure 10, respectively named “HRR Fuel” and “HRR Fuel FDS”.

In sum, as long as the fire acts in an enclosed space, it is ventilation-controlled and the previously used HRR versus time curve are no longer valid. Due to a lack of oxygen, a horizontal plateau will limit the HRR. In Eurocode 1 [24], Eq. (3) is proposed, the outcome of which is also depicted in Figure 10 (HRR EC1-1-2), together with the one calculated by Ozone (HRR Ozone). So, except for the fuel-controlled fire simulations, the fire load should be based on the shifted (by 8.33 min = 500s) Ozone HRR which is almost the same as the one of EN 1991-1-2.

#### 4.4.3 Parameters investigated in the FDS model

Default settings of FDS were used except for the items discussed hereafter.

**Geometry of the fire load.** Based on [27], where a simplified predefined heat release rate pro unit area (HRRPUA) is provided, several simulations were presently done, in which the geometry of the fire together with the condition which control the fire (fuel or ventilation) leads to different HRRPUA are as follows:

- For a crib under the condition of a fuel-controlled fire:  
 $22458 / [4 \cdot 15 \cdot 10 \cdot (1.5 + 2.0) \cdot 4 \cdot 0.05] = 54 \text{ kW/m}^2$ ,  
since cribs are supposed to burn on four sides.
- For a crib with a ventilation-controlled fire:  
 $4450 / [4 \cdot 15 \cdot 10 \cdot (1.5 + 2.0) \cdot 4 \cdot 0.05] = 10.60 \text{ kW/m}^2$ ,  
under the same conditions as above.
- Pro pile for a ventilation-controlled fire:  
 $4450 / [4 \cdot (1.5 \cdot 2.0 + 2 \cdot (1.5 + 2.0) \cdot 1)] = 111.25 \text{ kW/m}^2$ ,  
it is assumed that the burning face corresponds to the top and the four sides.

**Window breaking.** In section 3.1, it was shown that  $O$  is rather low and could impact the fire development. For that reason, several fire glass-breaking scenarios were investigated:

- With no glass at all (upper bound), please refer to the next section regarding the thermocouple devices.
- With the glass consisting of an upper (from 1.4 till 1.8 m) and lower part (from 1.0 to 1.4 m) and breaking at a temperature of 250°C (the temperature being controlled at 0.05 m out of the centre of each part out of the glass towards the fire).
- Same as above. At this moment, a simple temperature device is no longer used but instead a thermocouple device is. The difference between these two will be discussed in the next section regarding the thermocouple devices.

**Mesh size.** For the models with cribs of 5 by 5 cm, a mesh size of 5 cm in all directions is used which can be doubled or tripled (going up to 0.15 m) when a pile is considered. The latter value was kept as the maximum value due to the size of the roof girders (the height of which is 0.15 m). In the simulation, a perfect cubic mesh geometry was used.

**Thermocouple devices.** Since no specification about the used devices could be found in [17], traditional temperature devices measuring the temperature of the gases were firstly included in the first two models. In [11] however, it is mentioned that k-type thermocouples were used, which is why thermocouples were used in the subsequent simulations. The default setting parameters for an FDS thermocouple were used (i.e. diameter 1 mm, emissivity 0.85, density 8909 kg/m<sup>3</sup> and specific heat 0.44 kJ/kg/K for nickel).

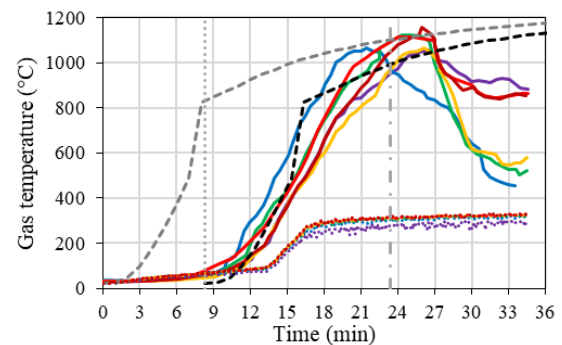
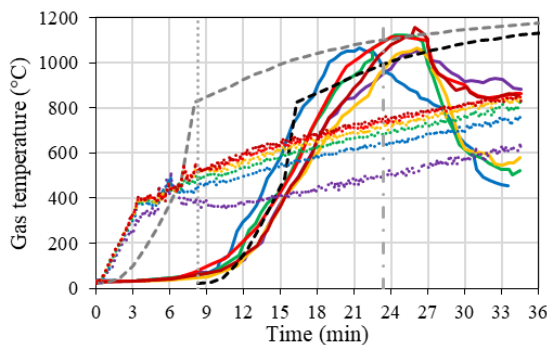
#### 4.4.4 Results

Eight simulations were conducted in total, as highlighted in Table 2 and presented in Figure 11 and Figure 12. One can find, in order of appearance, the type of HRR: simplified model based on measurements of time and temperature (fuel-controlled) or the so-called shifted Two-Zone Ozone model (ventilation-controlled); the fire load: cribs or pile; the scenario of window openings: (a) completely open from the start, (b) one glass panel or (c) failure in two steps; the type of temperature measurement devices : T = Temperature and TC = thermocouple device (including radiative part); and, last, the mesh size (Mesh) in [m]. Three time-related information are provided too; the simulation time (stopped after about 35 minutes), the average of the achieved simulation time in seconds per day and the total simulation time needed in days.

The first model cannot capture in a proper way the delay of the ignition or the temperature development because of the limited ventilation conditions which are presently not properly modelled. In the second model, thanks to the shifted HRR, a better approximation of the start of the fire is obtained. However, the opening scenario (c) leads to heavily fluctuating temperatures. Simulating the fire load using solid volumes instead of cribs delivers better results. The temperatures are well predicted till roughly 500°C. Changing to one glass panel does not influence the results. A sensitivity study for the mesh size is included by comparing the results of the simulations #4 (0.05 m), #5 (0.10 m) and #7 (0.15 m). Based on the results presented in Figure 11, for the thermocouple tree A# and for a mesh size of 0.15 m, the temperatures at position 2 (indicated as TA-2, blue dotted line) start to deviate. Therefore, a mesh size of 0.10 m seems to be the optimal choice.

Table 2 Overview of FDS models

#	HRR	Fire	Window	Dev.	Mesh (m)	Time (min)	CPU (min/day)	CPU (days)
1	Meas.	Cribs	(a)	T	0.05	35.9	0.15	227
2	Ozone	Cribs	(c)	T	0.05	35.5	0.38	93
3	Ozone	Pile	(c)	T	0.05	35.5	0.45	80
4	Ozone	Pile	(b)	TC	0.05	35.3	0.37	98
5	Ozone	Pile	(b)	TC	0.1	35.0	4.38	8
<b>6</b>	<b>Ozone</b>	<b>Pile</b>	<b>(a)</b>	<b>TC</b>	<b>0.1</b>	<b>35.0</b>	<b>4.38</b>	<b>8</b>
7	Ozone	Pile	(b)	TC	0.15	35.0	35.0	1
8	Meas.	Pile	(b)	TC	0.15	35.6	17.8	2



Simulations #1 and #2



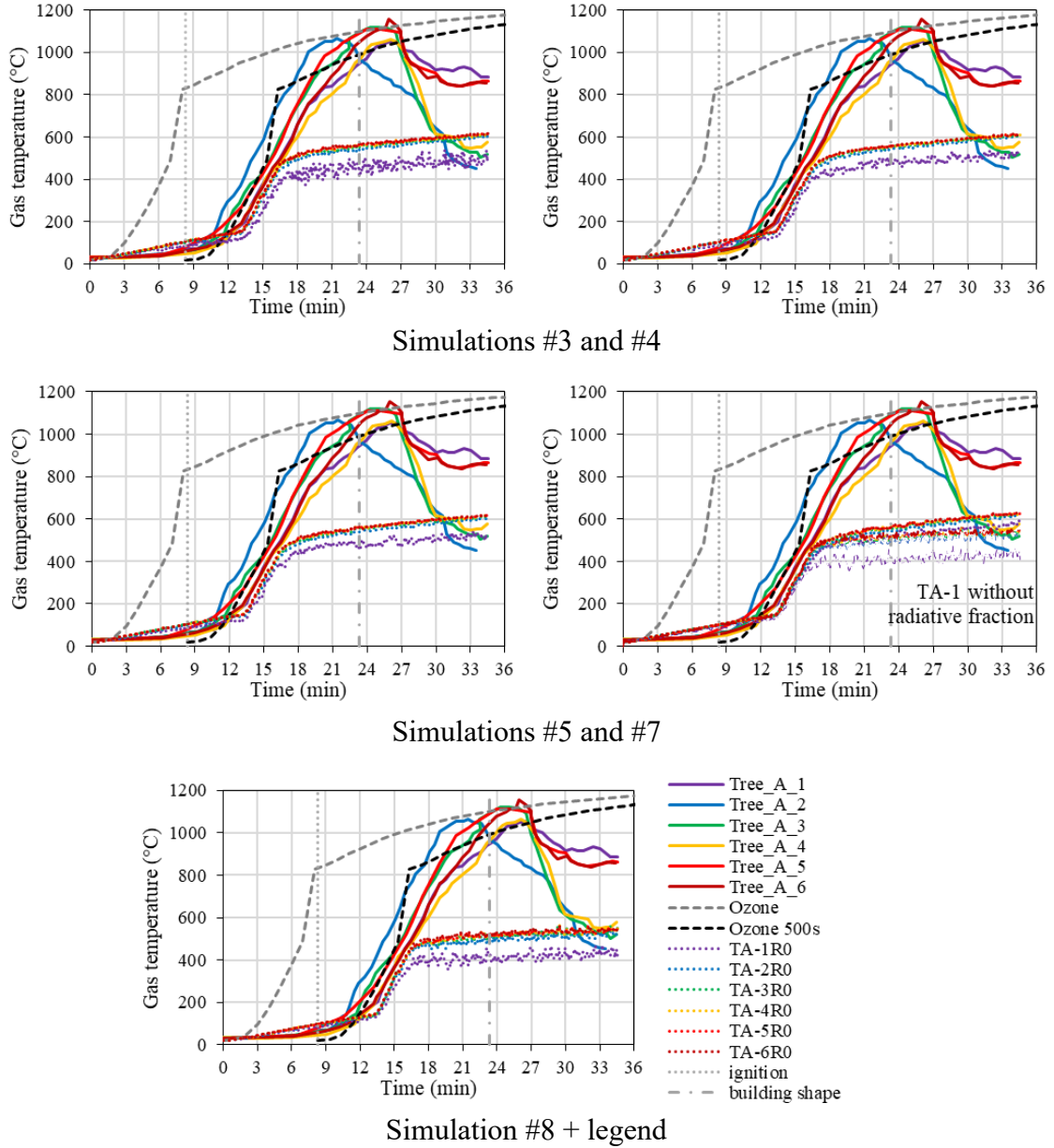
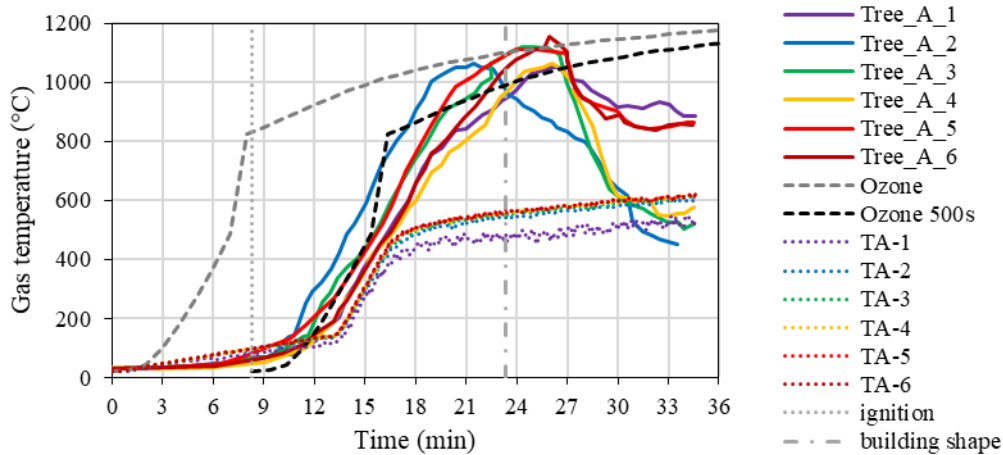


Figure 11. Temperature measurements, Ozone and FDS

The simulation #7 was also re-executed without radiation instead of the default FDS parameter (i.e. 0.35 for the radiative fraction which in fact is valid for hydrocarbon fuel). The results of this simulation are added in Figure 11 – Simulation #7. It is seen that this has very little influence on the fire development and that, beside thermocouple TA-1 ( $\Delta\theta \approx 180^\circ\text{C}$ ) which is close to the burning material, the temperature differences are very little ( $\Delta\theta < 60^\circ\text{C}$ ).

It should be noted that, if the HRR is calculated with glass breaking, it is redundant to include the window in the simulation. Hence, the next simulation, was done with an open window (scenario (a)) from the start. In Figure 11, the six measured temperatures of tree A# are provided together with the original and shifted Ozone simulation in grey and black dashed lines respectively. The FDS calculated gas or thermocouple temperature are provided as dotted lines, for all the simulations except simulation #6 which is provided in Figure 12. Out of the latter, one can notice that FDS, Two-Zone Ozone and the experiment itself deliver comparable results until about  $450^\circ\text{C}$ . The simulation #6, though delivering the best agreement with the measured results, is however not able to capture the post-flashover behaviour in an accurate way. The obtained temperatures remain at about  $400^\circ\text{C}$  too low compared to the test or to the Two-Zone Ozone results. Solving energy and mass equations for such

a large compartment fire (compared to the cell size) is probably causing the large discrepancy, however this should be properly and more thoroughly investigated. It is without discussion an appropriate tool for detailed analysis but not useful to simulate this experiment. Also the authors of [4] reported that, for a posteriori simulations, errors in the range of 10 to 50% for the hot layer temperature and 20 to 200% for the field values were calculated. Compared to the two-zone model, the FDS simulation provides inaccurate results in terms of temperature development within the compartment. Regarding to the amount of information that is needed and the CPU-time, this kind of simulations is not appropriate for a quick thermal analysis which is needed in the case of post-fire simulations.



**Figure 12. Temperature measurements, Ozone (dashed lines) and FDS (dotted lines) for ventilation-controlled, pile fire without glass panel and 0.10 m mesh size (i.e. simulation #6)**

## 5 REAL FIRE CASE-STUDY

### 5.1 Tigro fire

In 2018, a fire took place in the production area of the company Tigro in Pelt (Belgium). The main activity of the production site is filling small baskets with a product taken out of a large container. Filling is done in masonry bunkers (topped by a concrete slab), as can be seen in Figure 13 (a). The left bunker on this picture is where the fire ignition took place and where a local fire developed.

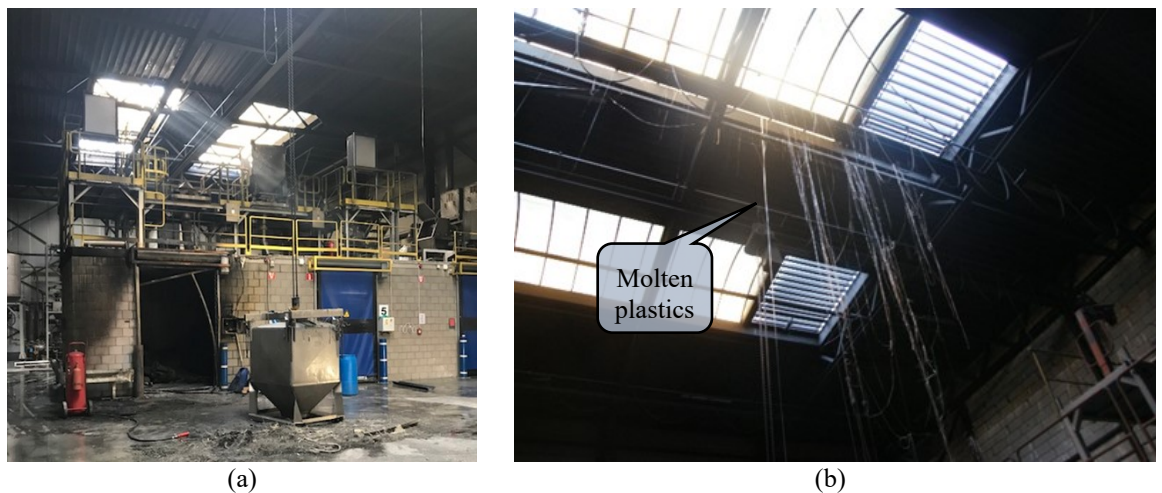


**Figure 13. View on the production area after fire a) masonry bunker; b) detail of roof light**



### 5.1.1 Geometry and materials.

As shown in Figure 14, in the past, the steel structure's height had been increased using a truss beam. The total width of the building between the outer flanges of the IPE330 profile columns is equal to 19.71 m while the roof ridge is 10.74 m above the foundation (which is also the ground floor level in this case). As in the Tongji experiment, the floor is made of concrete, masonry concrete blocks are used for the walls of the bunker whereas its roof (inside the steel hall) is made of concrete. Standard material characteristics were collected in the literature and are presented in Figure 14. Convection coefficients should be taken equal to 35 and 9 W/m<sup>2</sup>K for the hot and cold surface respectively.

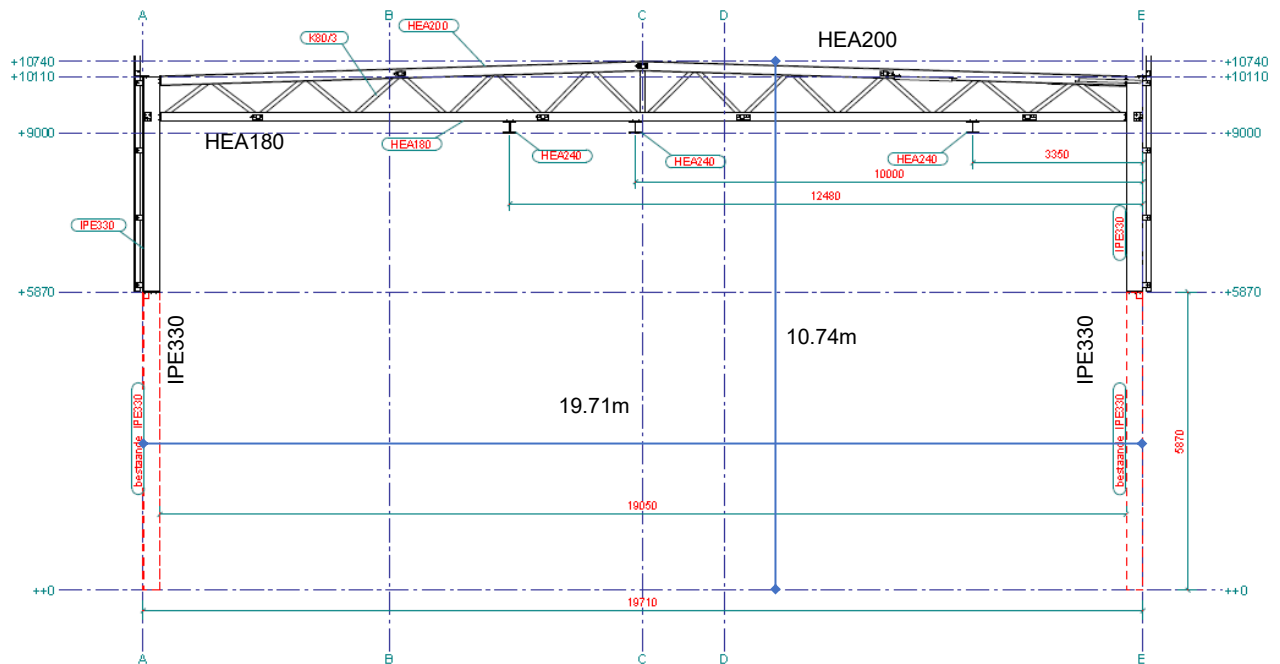


Figure 14. Section of the Tigro building

The bunker can be described as an enclosed volume with L x B x H equal to 4.5 x 4.8 x 3.6 m<sup>3</sup> with a door width of 1.8 m (full height) in the widest part of the so-called sub compartment. It can be seen out of the presented pictures that the structure survived the fire. The fire remained in a localised area due to the bunker enclosures and only the roof beam was trapped in a hot smoke layer. On Figure 13 (b), the melted skylights and cable insulation, as well as opened smoke evacuation system can be seen. According to the fire brigade, the whole internal volume was filled up with smoke, however no flames came out of the skylights.

Table 3 Material characteristics

Description	Material	Thickness (m)	Conductivity (W/mK)	Spec heat (J/kgK)	Density (kg/m <sup>3</sup> )	Material emissivity
Floor	Concrete	0.15	1.6	1000	2300	0.8
Masonry wall	Concrete blocks	0.14	1.2	1000	2000	0.8

After a real fire, it is always useful to look for some valuable temperature indicators. Note that the following material temperatures are denoted  $\theta$  as opposed to T which is the output temperature in Ozone. In this case-study, the polycarbonate roof skylights were melted so  $\theta_{glass}$  is higher than 160-180°C. However, the aluminium (EN AW 6061T6) strips in between the polycarbonate windows remained intact; the maximum temperature of the hot smoke layer can thus be estimated as ranging

between 180 and 230 °C. The latter temperature is based on  $\theta_{\eta;fi,Al}$  equalling 229°C choosing the reduction factor of the load ratio  $\eta_{fi} = 0.65$  and an unstrained member analysis [28]. It is worth noting that the corresponding critical steel temperature for an unstrained member analysis [25]  $\theta_{crit}$  is 540°C (based on the same load ratio), this temperature can be found in the next figures.

### 5.1.2 Spatial model of the local fire

Each of the following simulations will be done under the assumption that the HRR can be described by 500 kW/m<sup>2</sup> which is the maximum rate for a fuel-controlled fire according to EN 1991-1-2. For the Two-zone model, the assumption is that  $t_a$  is 150 s (2.5 min) i.e. it is the time needed to achieve a HRR of 1 MW with a quadratic growing rate, as indicated in Annex E of [24]. The door opening is so large that the fire is assumed to be fuel-controlled in the sub compartment. As fire load the 0.01 m finishing from walls and ceiling was taken with a density of 850 kg/m<sup>3</sup> and a calorific value of 30 MJ/kg (polyester) or 20930 MJ and an additional 204 MJ of the filling product itself.

Two local fire approaches to determine the time-temperature relationships will be considered see Figure 16, but they first need to be validated by the aid of the observations:

- The Heskestad fire model with the temperature along the vertical axis in the flame plume  $\theta(z)$  according to Annex C of [24] with an equivalent pool diameter corresponding to the floor area of the bunker.
- The same Heskestad fire model with an equivalent pool diameter corresponding to the door area of the bunker and the same maximum fire density as before.

Both approaches deliver a distribution of the smoke temperature over the building height. Looking to the observed damage to the top of the bunker (Figure 13), it seems that the first scenario (a) delivers the best fit with the reality. Seeing that the smoke temperature reaches 223 °C or 319°C at the ridge level respectively for the scenario (a) or (b).

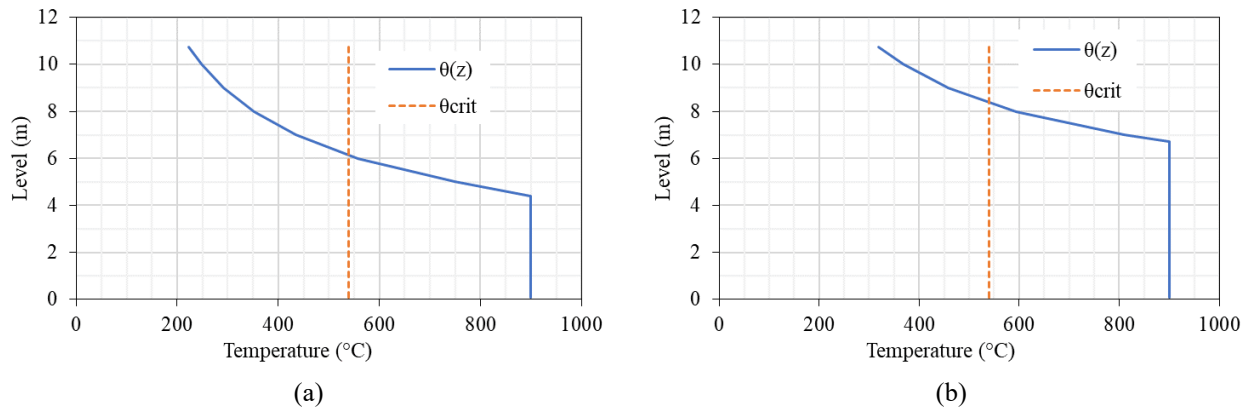


**Figure 15. Local fire approach (a) floor surface of the bunker and (b) door surface of the bunker**

Seeing that the aluminium strips in between the polycarbonate windows remained intact, the scenario (a) delivers the best match. For this scenario, the maximum temperature reached by the top profile of the truss beam is 217°C while it is 268°C for the bottom profile. The critical steel temperature  $\theta_{crit} = 540^\circ\text{C}$  (corresponding to the recommended reduction factor of 0.65 in [25]) is also shown in these figures.

### 5.1.3 Two-zone time-dependent model

A Two-zone model using Ozone [29] was considered for the temperature development in the bunker (considered as sub-compartment). It is provided in Figure 16 in function of time, for a hot top- (TU) and cold bottom (TL) layer (until the fire develop into a one-zone fire). In the corresponding figure, the ISO834 temperature-time curve is also given as reference. Again, the critical steel temperature  $\theta_{crit}$  is mentioned.

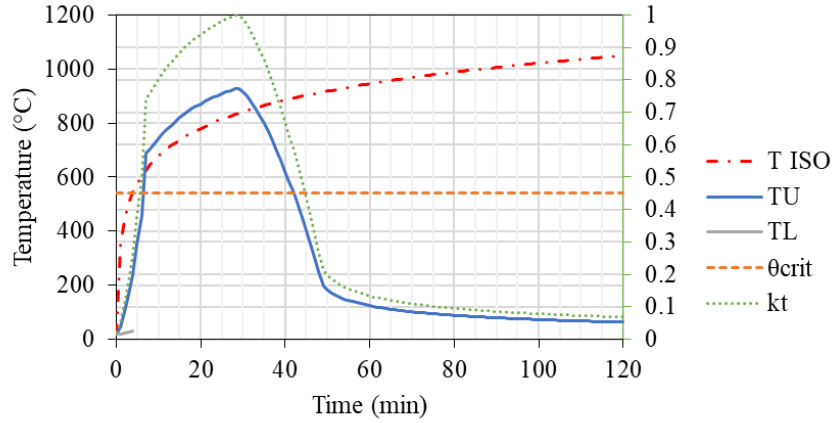


**Figure 16. Predicted temperature profiles in the filling bunker in function of time and proposed time scaling factor  $k_t$**

As the purpose is to investigate the effect during heating and cooling of the bay, a combination of the time dependent Two-zone model approach with the spatial distribution of the Heskestad fire model is used. To do so, in a first step, a time dependent scaling factor  $k_t$  is proposed by scaling the values obtained in Figure 16 by the maximum obtained temperature  $T_{max}$ . Reference should be made to the right vertical axis in Figure 16 and the dotted line representing  $k_t$  both plotted in the same colour. In a second step, the evolution of the local fire temperature depending on the height (Figure 15 (a)) is now weighted by the time scaling factor  $k_t$  and applied to the elements of the truss beam. This is assumed reasonable as the whole upper part of the hall was filled with a smoke layer presumed to be of a constant temperature equal to the one of the centre of the flame plume.

#### 5.1.4 Results compared to observations

This relatively straightforward method is easy to apply and delivers accurate results for the post fire evaluation. This can be achieved with a combination of a level depending local fire and time dependency sub-compartment fire. Limited observations done after the fire from non-structural components allow to update the model and deliver consistent results which can be used to explain other damage patterns or temperature reached in other structural parts. It also allows to assess the structural behaviour after the fire (remaining strength and reliability) as presented in the next sections of this paper.

#### 5.1.5 Locked-in forces

With the methodology presented above, it was possible to numerically expose the portal frame with its truss beam to the real fire. Out of plane deformations are blocked by spacers and fixations to wall panels. Particularly, the temperature difference between the upper (top) and lower (bottom) truss beam were included. As an approximation however, the diagonals were subjected to the same temperature as the upper truss beam. A simulation of the heating and cooling was performed through SAFIR® [30] in combination with the Eurocode 3 material model for S235 carbon steel and with permanent loads acting on the structure. During the exposure to elevated temperatures, plastification of some diagonals was observed. After cooling down the structure for 120 minutes, locked-in forces in the structure could be calculated, more specifically in the diagonals closest to the column, as indicated in Figure 17. For the tension bar, for example, the load increased by 25%. This is due to structural restraints and unequal heating of the top and bottom beams.

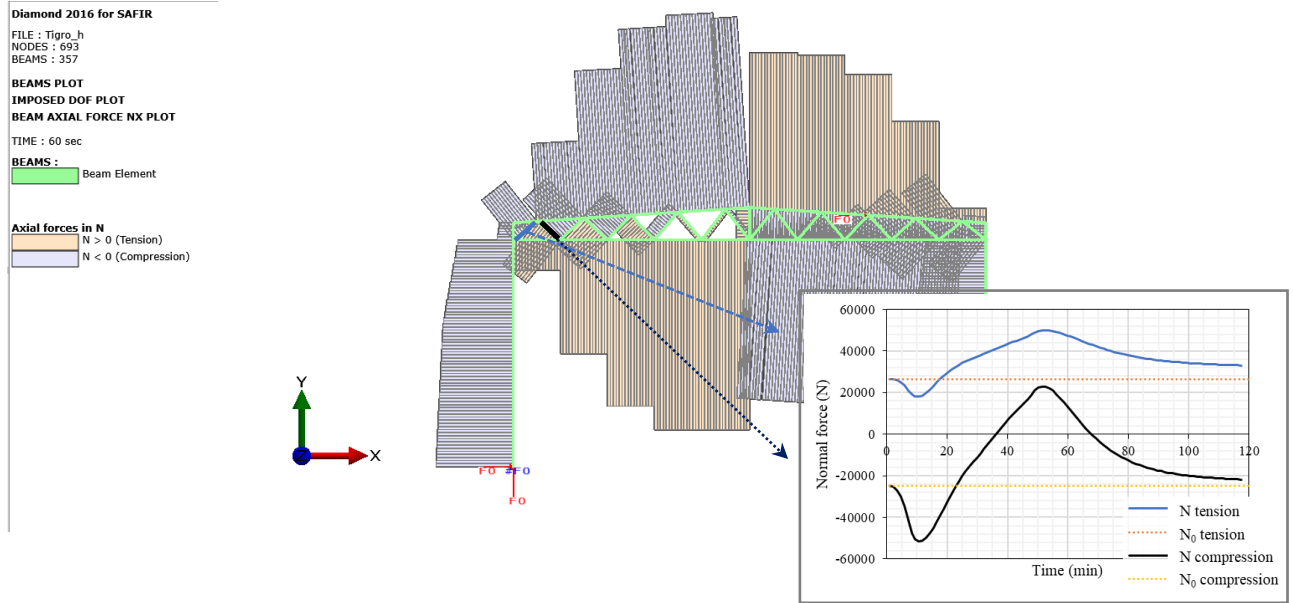


**Figure 17. Normal forces diagram after the fire their evolutions in bars 334 and 330.**

To verify the influence of the locked-in forces on the bearing capacity, the initial structure (i.e. without locked-in forces) was loaded in ambient conditions with the same dead loads, i.e. a uniformly distributed load was applied on the upper truss bar, linearly increasing to the dead load (1.25 kN/m) in 20 s, followed by an additional superimposed load linearly increasing with 25 kN/m in 250 s (4.17 min). The time history of the loads is presented by a dashed line in Figure 18 (“load history ambient” - right reading axis) together with the temperature history of the top (and diagonal) and bottom chords (left reading axis).

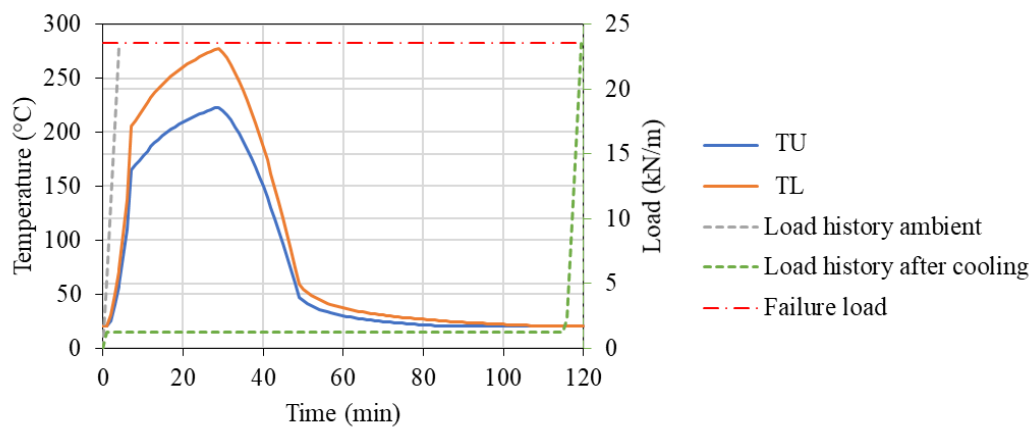


**Figure 18. Time history of applied temperatures and loads on top beam**

In Figure 19, the failure mode is presented. It occurs after 243 s (4.05 min) i.e. when the total load acting on the upper beam equals to  $1.25 + (243 - 20) / 250 \cdot 25 = 23.54$  kN/m. The failure mode is initiated by buckling of the first and third diagonal, as indicated in the right deformed Figure 19.

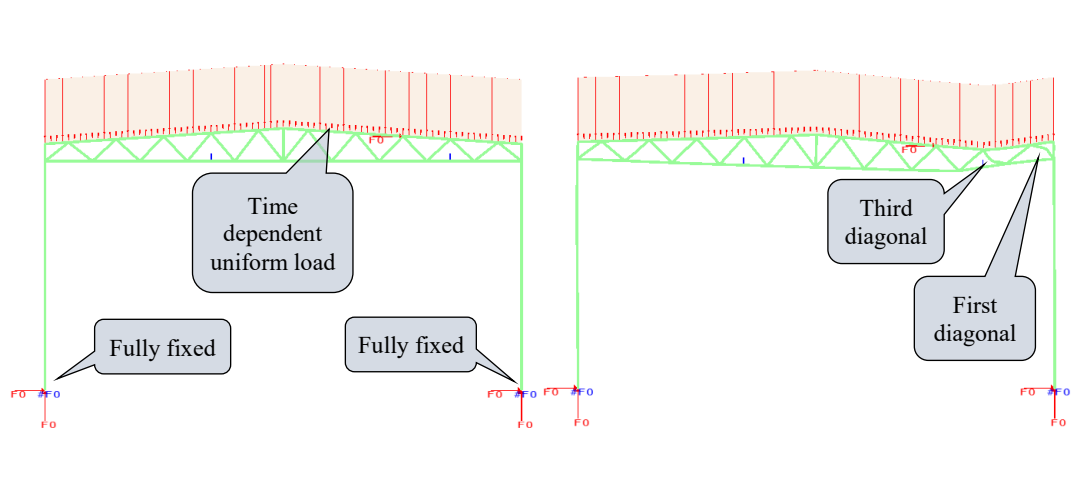


**Figure 19. Portal frame, supports, concentrated loads (blue) and user defined load function (orange) in ambient conditions and failure mode at the right.**

The cooled-down structure (i.e. with its locked-in forces) was then also loaded up to failure, see again Figure 18 “load history after cooling”. It can be seen that the top chord uniformly distributed dead load is increasing to 1.25 kN/m during the first 20 s and that then a superimposed load of maximum 25 kN/m is developing during the upcoming 250 s (4.17 min). Collapse happens after about 7173 s (119.55 min) at a load equal to 23.54 kN/m, at the same failure load as before. The failure mode is shown in Figure 20 and exactly the same as before (i.e. Figure 19). It can therefore be concluded that for such structures, the locked-in forces have negligible influence on the structure behaviour after the fire.

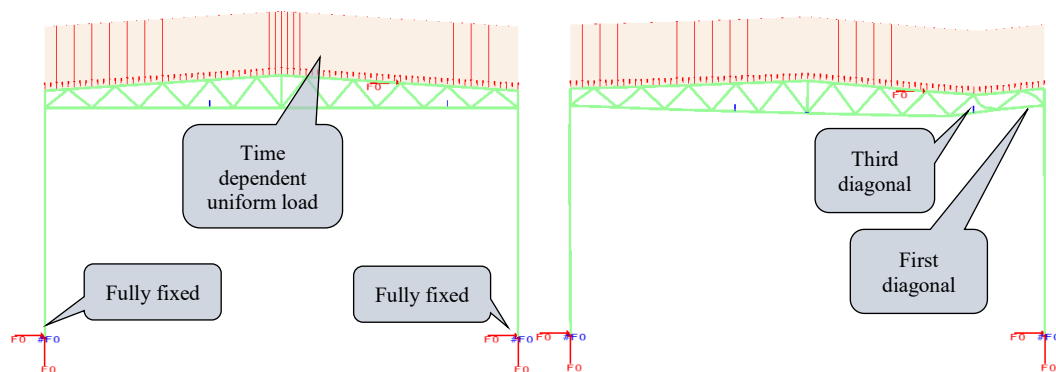


**Figure 20. Portal frame, supports, concentrated loads (blue) and user defined load function (orange) and failure mode after exposure to a natural fire and cooling down at the right**

## 5.2 Truck-centre fire

In 2017, a fire took place in a truck centre in Beringen (Belgium). According to the fire brigade, the burning lasted for quite a long period and hot smoke extended into the whole workshop just when the fire was discovered. Nine trucks were damaged as was the structure itself. However, it was not possible to visually detect damages to the main steel structure or to the cold-formed sigma girders (made of S320 or S350 steel). Dog-bone coupons were taken out of the wind bracing and tested in tension in the Construction laboratory of the Civil Engineering department at KU Leuven, Campus De Nayer. Based on the results and inspection of the structure, it was decided to re-use it and, today, it is still in operation.





**Figure 21. Truck centre after fire and removal of the trucks and equipment (left) and fire source (right)**

### 5.2.1 Geometry and materials.

This industrial building has a length of 60 m and 2 bays of 12.5 m each with a double pitch roof (10% slope) and 11 portal frames each 6 m. It is well optimised: the roofbeams are made of IPE220 profiles, 5.10 m outer columns made of IPE240 profiles (starting at +0.30m) while the 6.95m columns in centre of the frame are made of HEA180 profiles (starting at -0.30m). The roof ridge is at 6.85m and the roof edge at 5.60m, all levels above the finished level of the workshop.

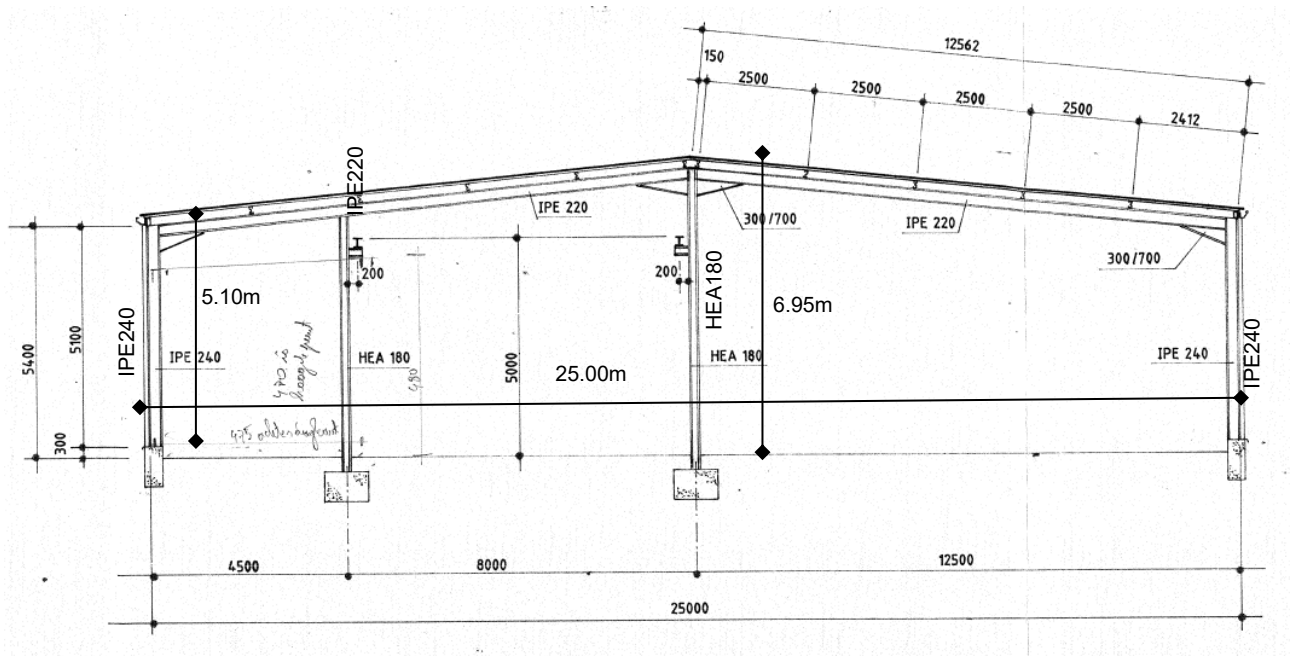


**Figure 22. Section of the Truck Center**

Insulation blanket material (estimated weight =  $0.04 \text{ kN/m}^2$ ) was used in the roof whereas, for the façades of the end walls, sandwich panels were used. As the insulation blanket material in the roof was composed of mineral wool packed in between two thin aluminium foils, it melted quickly. Therefore, only the steel sheet ( $0.75 \text{ mm}$  – weight =  $0.07 \text{ kN/m}^2$ ) was taken into account in the

simulation. The side walls were mostly composed of non-insulated gates, hence a mean insulation thickness of only 2 cm was considered. In the roof, eight PVC single layer semi-transparent 1 m wide skylights were incorporated, the width of which was 25 m.

A stepwise opening scenario was chosen for the skylight with 10% opening under ambient conditions, 50% at 80°C followed by 100% at 120°C. As there were fourteen gates, of dimensions 4.40 m by 4.37 m, it was assumed that 1 gate was completely open at the start of the fire (corresponding to 7%), 2 gates at 200°C (14%) and 6 at 300°C (42%), considering a (bi-)linear increase between these limiting values. In Figure 21, it can be seen that the transparent polycarbonate door panels remained intact as the gas temperature was limited by 160-180°C. However, the PVC rooflights were burnt down. Standard material characteristics were collected from the literature and are presented in Table 4. Convection coefficients are taken equal to 25 and 9 W/m<sup>2</sup>K for the hot and cold surface.

**Table 4 Material characteristics**

Description	Material	Thickness (m)	Conductivity (W/mK)	Spec. (J/kgK)	heatDensity (kg/m <sup>3</sup> )	Emissivity
Floor	Concrete	0.15	1.6	1000	2300	0.8
End wall	Wool	0.10	0.037	1030	60	0.8
Blanket	Wool	0.06	0.037	1030	60	0.8
Roof sheet	Steel	0.0007	45	600	7850	0.8

The following design situations were investigated:

- Ultimate limit state in ambient condition – purlin: The loads are the purlin's weight = 0.05 kN/m<sup>2</sup>; the steel sheet's weight = 0.07 kN/m<sup>2</sup> and the maintenance load = 0.80 kN/m<sup>2</sup>, such that the design load becomes  $1.5 \cdot 0.8 + 1.35 \cdot (0.07 + 0.05) = 1.36 \text{ kN/m}^2$
- Ultimate limit state in fire condition – purlin: the design fire load is  $0.07 + 0.05 = 0.12 \text{ kN/m}^2$  which leads to a utilization ratio  $\mu_0 = 0.12/1.36 = 9\%$ . While table 4.1 of [25] prescribes a critical temperature of 350°C for cold-formed sections, this very low ratio allows temperatures to reaching 840°C. But even this temperature was exceeded if a the local fire scenario is assumed, which is the reason why the roof cover plated melted down above the fire source.
- Ultimate limit state in ambient condition – IPE220 beam profile: The loads are the IPE220 beam profile's weight 0.26 kN/m; the snow load (0.4 kN/m<sup>2</sup>) and technical equipment (0.20 kN/m) so that the design load becomes  $6 \cdot [1.5 \cdot 0.4 + 1.35 \cdot (0.07 + 0.05)] + 1.35 \cdot 0.26 + 1.5 \cdot 0.20 = 5.22 \text{ kN/m}$ .
- Ultimate limit state in fire condition – IPE220 beam profile: the design fire load is  $6 \cdot (0.07 + 0.05) + 0.26 + 0.20 = 1.18 \text{ kN/m}$  leading to a utilization ratio  $\mu_0 = 1.18/5.22 = 23\%$ . Based on [25], a critical temperature  $\theta_{crit}$  of 707°C can be calculated for this particular case.

### 5.2.2 Spatial model of the local fire

The origin of the fire could have been due to electric misconnections in one of the trucks, Figure 21 b). The fire remained local as the tyres at the back side of the aforementioned truck were not melted. The lowest fire load value of an unloaded truck according to NFPA 502 (2004) is about 20 MW, while an ordinary car represents only 5MW. For a partially burnt unloaded truck, one can presume a fire load of 10MW distributed on a surface of 2.4 by 1.2 m<sup>2</sup> which will herein be converted to a Ø1.92 m pool fire. The fire position is as in reality i.e. in the centre of the second bay at 1.25 m of the gate and at 0.5 m above the ground floor. At that point, the ceiling receives a heat flux of 47 kW/m<sup>2</sup> according to Annex C of [24] and, as was observed after the fire, the steel sheet disappeared (critical temperature about 350°C). The influence of the fire at the level of the ceiling can be tuned by changing the distribution surface, in the case of a surface of 7.26 by 4.75 m<sup>2</sup>, the heat flux attains 10 kW/m<sup>2</sup>, a value sufficiently low to avoid fire propagation due to radiation [31]. According to the observations

of this model, it seemed that the building and equipment located at about 3.5 m of the fire source were not ignited and that corresponds well to the latter assumption. It is worth noting that a simulation with the Heskestad spatial model, as for the Tigro case-study, is, in this case, no longer valid since the flames touched the ceiling. Nevertheless, using the values deduced above lead to a ceiling temperature of 900°C.

### 5.2.3 Two-zone model.

Out of the Belgian regulations for industrial buildings [32], it seems that the design fire load for a garage is equal to 300MJ/m<sup>2</sup>. A  $t_a = 300$ s (5 min) and HRR = 250 kW/m<sup>2</sup> are chosen to start with. With the previous boundaries and opening scenarios, A fully developed fire is obtained after only 20 minutes and, the temperature severely increases after 70 minutes, see Figure 23. It corresponds to the visual observations of the fire brigade who could start fighting the fire before high temperatures could develop.

A numerical maximum temperature of 724°C is reached after 77 minutes, however it was not the case in the real case-study. Indeed, observing the painting of the runway beams and principal structural elements, one realised that it was still intact next to the fire source.

To simulate one of the actions of the fire brigade (FB), all doors were opened and a second model was run, (see abbreviation FB in Figure 23). In this case, the temperature is always limited to 462°C, hence far below the critical temperature of the structural elements.

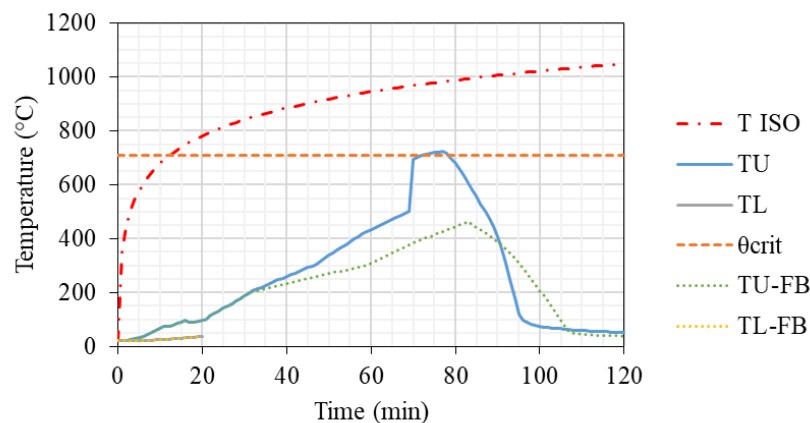


Figure 23. Predicted temperatures of hot gases in compartment

### 5.2.4 Comparison with observations and post fire material testing

After the fire, some straightness measurements of the structure are taken by a surveyor and it seems that the main portal frames are still (or again) straight and no damage could be observed which leads to the conclusion that the action of the fire brigade saved the structure.

To guarantee the client this statement, four dog bone coupons of 150 mm<sup>2</sup> were taken out of the flanges of one wind bracing made of a 50x50x5mm angle section. By back calculation, it was estimated that mild carbon steel S235 was used in the design, which was anyway commonly used when the frame was built. Figure 24 clearly shows that the steel characteristics remained unchanged with a quite high yield strength and a total elongation after rupture around 30%. The presence of a yield plateau, the still high yield strength and the remaining ductility clearly show that the material's characteristics were not influenced by the fire. After the external assessment of the structure was delivered, it was decided to replace girders for durability reasons seeing that their galvanised protection layer had been removed. It is known that this effect takes place starting from above 400°C.



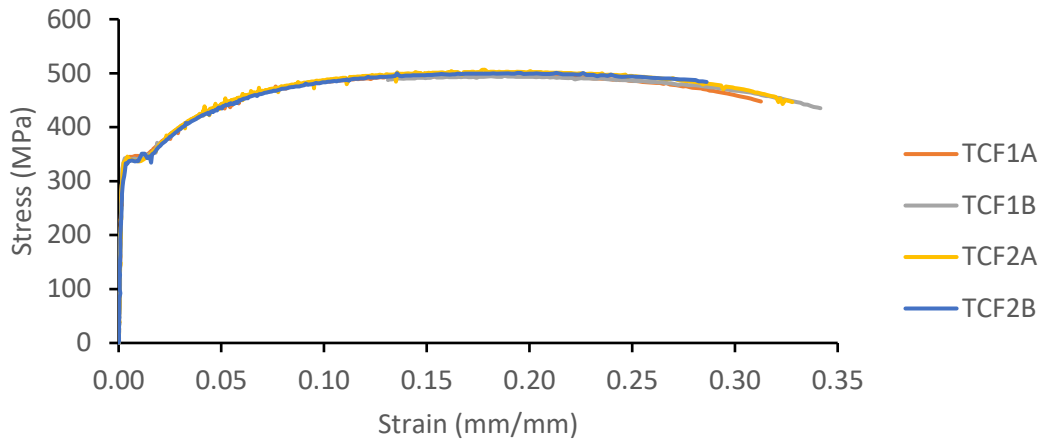


**Figure 24. Measured stress-strain curves after fire based on 4 coupons**

Despite the damage observed at the roof, observations (painting) from inside the compartment confirmed that the temperatures stayed in general relatively low. That the influence area was limited could be assumed out of the local fire approach and material testing confirmed the temperatures as simulated by the Ozone software.

## 6 CONCLUSIONS

In the present paper, the authors demonstrate that it is possible to obtain an accurate idea of the temperatures reached in the structural elements of a known steel building during and after the action of a fire by the use of the design models listed in the informative annexes out of EN 1991-1-2 [24]. Simulations of the effect of a real fire on three chosen industrial structures having been submitted to a parametric, local fire, two-zone model and CFD's are carried out. Those several techniques based on a number of assumptions are contemplated, from simple and rather straightforward ones to simulations using FDS.

The first experimental study concerns a steel portal frame which was subjected to an instrumented fire for which one has access to all the information during and after the fire [11]. Today, even though FDS is considered inappropriate to simulate flashover in large compartment fires, it still stays a powerful instrument to study more local effects. As such it can deliver valuable and helpful results for post fire assessment. It is indeed inappropriate in the sense that there is a clear unbalance between computational efforts and accuracy of the outputs. Through the FDS model, several features of the test can be thoroughly modelled to increase the accuracy of the results, however increasing the calculation time. Despite the sometimes immense required computing time, one herein demonstrated that the FDS model could predict the temperature development in a very accurate way, however, in this case, till a relatively limited temperature of about 450°C. One of the simplest FDS model delivers the best fit with the measured temperatures, i.e. using a solid burning volume and the least fine mesh. As mentioned in the paper, since the calculated heat release rate took the glass breaking into account, all openings were set open from the beginning of the simulation, without breaking scenarios. The Two-Zone model delivers quick and accurate results (time versus temperature development) especially if the model can be calibrated by the use of tests or based on visual observations reported by the fire brigade during the fire. The results are filling the gaps between what can be easily observed after the fire (or during, by the fire brigade) and what remains unknown. Looking towards time efficiency and accuracy, the Two-Zone model performed well, even till collapse of the building.

In addition, two additional real (i.e. non-academic) fires, after which the structure survived the fire, are studied by means of the same proposed methodology. A combination of the time dependent Two-zone model approach with the spatial distribution of local fire models is used. In the second case-

study, the evolution of the Two-zone model temperature is scaled to the maximum temperatures initially calculated with the chosen local fire model. This is proven practical and successful. For the three presented case-studies, a number of information and visual observations (as well as full-scale measurements in the first case) are available and used to compare the numerical and real temperature versus time curves reached in the structure.

This kind of simulations is extremely important to relatively quickly assess the remaining load-bearing capacity of the structure based on the post fire material characteristics. When the structure still stands – which is often the case for steel structures – and when the deformations are not jeopardising the building's serviceability, decisions have to be taken quickly to avoid unnecessary delays during which the industry can no longer carry out its business. Nevertheless, some important results can be uncovered by the analysis (such as the presence of locked-in forces) the effect of which on the structure's post fire failure load must be carefully investigated.

Based on the present research, it is shown that a combination of a parametric fire or two-zone models and a local fire approach can deliver an accurate simulation of the temperature distribution over the fire period. However, there is a clear need to update the models against a series of information collated on site and/or visual observations provided by the fire brigade. Also, such simulations need prior knowledge of the heat release rate pro unit area which is, in most cases, possible to assess based on the inspection of the building after the fire.

## REFERENCES

- [1] Q. Guo en A. E. Jeffers, „Finit-element reliability analysis of structures subjected to fire,” *Journal of structural engineering*, pp. 1-11, 2014.
- [2] J.-M. Franssen, „Evaluatie van de stabiliteit na een brand: de vuurproef,” *Fire Forum Magazine*, nr. 63, pp. 16-19, 2018.
- [3] G. Rein, J. L. Torero, J. Wolfram, J. Stern-Gottfried, N. L. Ryder, S. Desagher, M. Lazaro, F. Mowrer, A. Coles, D. Joyeux, D. Alvear, J. A. Capote, A. Jowsey, C. Abecassis-Empis en P. Reszka, „Round-robin study of a priori modelling predictions of the Dalmarnock Fire Test One,” *Fire Safety Journal*, nr. 44, pp. 590-602, 2009.
- [4] G. Rein en J. Wolfram, „Model benchmarking the growth phase of Dalmarnock fire test one,” in *Benchmark studies: Experimental validation of numerical models in fire engineering*, Prague, CZ, COST CTU Publishing House, 2014, pp. 134-146.
- [5] M. Ada, N. Yüzer en Y. Ayvaz, „Postfire damage assessment of a RC factory building,” *ASCE Journal of Performance of Construction Facilities*, nr. 33, pp. 1-12, 2019.
- [6] T. Molken, „FDS versus EN-models: A comparison between the Heskestad model from EN and CFD results,” *Journal of Structural Fire Engineering*, vol. 6, nr. 3, pp. 185-195, 2015.
- [7] T. Molken, R. Van Coile en T. Gernay, „Assessment of damage and residual load bearing capacity of a concrete slab after fire: Applied reliability-based methodology,” *Engineering Structures*, nr. 150, pp. 969-985, 2017.
- [8] T. Molken en B. Rossi, „Modelling Real Fire by FDS and 2-Zone Model for Structural Post-Fire Assessment,” in *Advances in Fire Safety Engineering*, Porto, Springer Nature Switzerland AG, 2019, pp. 48-60.
- [9] B. Merci en T. Beji, *Fluid Mechanics Aspects of Fire and Smoke Dynamics in Enclosures*, Leiden: CRC Press, 2016.

- [10] T. Molken en F. Hanus, „Contribution of Non-structural Concrete Walls to the Fire Resistance of Unprotected Steel Frames,” in *Applications of Structural Fire Engineering*, Dubrovnik, 2015.
- [11] G. Lou, C. Wang, J. Jiang, Y. Jiang, L. Wang en G.-Q. Li, „Experimental and numerical study on thermal-structural behavior of steel portal frames in real fires,” *Fire safety Journal*, nr. 98, pp. 48-62, 2018.
- [12] L. Pyl, L. Schueremans, W. Dierckx and I. Georgieva, “Fire safety analysis of a 3D frame structure based on a full-scale fire test,” *Thin-Walled Structures*, no. 61, pp. 204-212, 2012.
- [13] C. Thauvoye, P. Russo, J.-M. Blanchet, S. Duplantier, J. Kruppa, A. Muller, S. Patej, J. Taveau en B. Zhao, „Method for calculating heat fluxes from a warehouse fire,” in *8th International conference on Performance-Based Codes and Fire Safety Design Methods*, Lund, 2010.
- [14] M. Mensinger, P. Schaumann, P. Kraus en F. Tabeling, *Optimierter Einsatz intumeszierender Anstriche im Stahlbau IGF 17200 N*, Düsseldorf: Deutscher Ausschuss für Stahlbau, 2012.
- [15] M. Mensinger en P. Kraus, „Optimierter Einsatz reaktiver Brandschutzsysteme im Stah- und Verbundbau,” *Verlag für Architektur und technische Wissenschaften*, nr. 84, pp. 10-18, 2015.
- [16] T. Molken, „Damage Control of Intumescent Painting,” in *Application of Structural Fire Engineering*, Prague, 2013.
- [17] B. Zhong, Y.-Q. Jiang en G.-B. Lou, „Experimental study on the thermal and structural responses of a full-scale steel structure under natural fire,” in *The 10th international conference on Structures in Fire*, Belfast, 2018.
- [18] K. McGrattan, S. Hostikka, R. McDermott, J. Floyd en M. Vanella, *Fire Dynamic Simulator; User's Guide*, Maryland: NIST & VTT, 2018.
- [19] EN 1991-1-2:2002/AN-LU:2011, Luxemburg national annex to Eurocode 1: Actions on Structures - Part 1-2: General actions - Actions on structures exposed to fire, Luxembourg: ILNAS, 2011.
- [20] Y. Wang, Q. Wang, G. Shao, H. Chen, J. Sun, L. He en K. Liew, „Experimental study on critical breaking stress of float glass under elevated temperature,” *Materials and Design*, vol. 60, pp. 41-49, 2014.
- [21] A. H. Buchanan en A. K. Abu, *Structural design for fire safety*, 2nd red., Chichester: John Wiley & Sons Inc., 2017.
- [22] S. Reitgruber, C. Pérez-Jimenez, C. Di Blasi en J.-M. Franssen, „Some comments on the parametric fire model of Eurocode 1,” Jordanstown, 2006.
- [23] JCSS, „Probabilistic Model Code,” <https://www.jcss.byg.dtu.dk>, Denmark, 2001.
- [24] EN 1991-1-2, Actions on structures - Part 1-2: General actions - Actions on structures exposed to fire, Brussels: CEN, 2002.
- [25] EN 1993-1-2, Design of steel structures - Part 1-2: General rules - Structural fire design, Brussels: CEN, 2004.
- [26] J.-F. Cadorin, D. Pintea, J.-C. Dotreppe en J.-M. Franssen, „A tool to design steel elements submitted to compartment fires - Ozone v2 Part2: Methodology and application,” *Fire Safety Journal*, vol. 5, pp. 429-451, 2003.
- [27] J. Degler, A. Eliasson, J. Anderson, D. Lange en D. Rush, „A-priori modelling of the Tisova fire test as input to experimental work,” in *ASFE*, Dubrovnik, 2015.
- [28] EN 1999-1-2, Eurocode 9 - Design of aluminium structures - Part 1.2 : Structural fire design, 2009 red., Brussels: CEN250, 2007.
- [29] J. Cadorin en J. Franssen, „A tool to design steel elements submitted to compartment fires - OZone V2. Part 1: pre- and post-flashover compartment fire model,” *Fire Safety Journal*, vol. 5, nr. Vol. 38, pp. 395-427, 2003.

- [30] J. Franssen en T. Gernay, „Modelling structures in fire with SAFIR,” *Journal of Structural Fire Engineering*, vol. 8, nr. (3), pp. 300-323, 2017.
- [31] J. Hare en G. Burrell, Review of HSE building ignition criteria., Buxton: HSL/2006/33 Health and Safety Laboratory, 2006.
- [32] ibz, De klasering van industriegebouwen, Brussel: Federale Overheidsdienst Binnenlandse Zaken, 2011.